ACS Photonics

Article

pubs.acs.org/journal/apchd5

Plasmon-Assisted Photoresponse in Ge-Coated Bowtie Nanojunctions

Kenneth M. Evans,[†] Pavlo Zolotavin,[‡] and Douglas Natelson*[,‡,§]

[†]Applied Physics Graduate Program, [‡]Department of Physics and Astronomy, and [§]Department of Electrical and Computer Engineering, Rice University, Houston, Texas 77005, United States

ABSTRACT: We demonstrate plasmon-enhanced photoconduction in Au bowtie nanojunctions containing nanogaps overlaid with an amorphous Ge film. The role of plasmons in the production of nanogap photocurrent is verified by studying the unusual polarization dependence of the photoresponse. With increasing Ge thickness, the nanogap polarization of the photoresponse rotates 90°, indicating a change in the dominant relevant plasmon mode, from the resonant transverse plasmon at low thicknesses to the nonresonant "lightning rod" mode at higher thicknesses. To understand the plasmon response in the presence of the Ge overlayer and whether the Ge degrades the Au plasmonic properties, we investigate the photothermal response (from the temperature-dependent Au resistivity) in no-gap nanowire structures, as a function of Ge film thickness and nanowire geometry. The film thickness and geometry dependence are modeled using a cross-sectional, finite element simulation. The no-gap structures and the modeling confirm that the striking change in nanogap polarization response results from redshifting of the resonant transverse mode, rather than degradation in the Au/Ge properties. We note remaining challenges in determining the precise mechanism of photocurrent production in the nanogap structures.

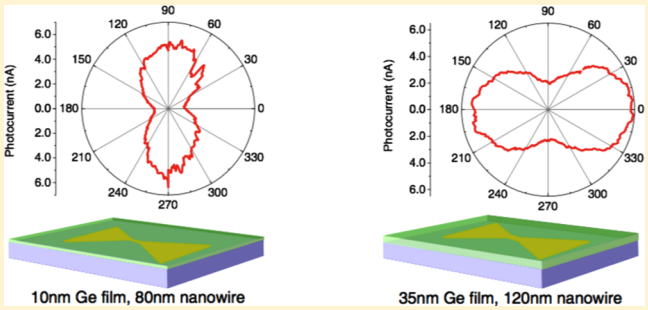

KEYWORDS: *plasmonics, optoelectronics, nanogap, polarization*

Light coupled into surface plasmons in metallic nanostructures can generate extremely large enhancements to the local electromagnetic field. Optical antennas exploit the resonant behavior and large scattering cross section of plasmons in nanostructured metals for use in a wide variety of applications, including surface-enhanced Raman spectroscopy (SERS),[1,2] subwavelength optics,[3,4] plasmonic optical trapping,[5−8] and plasmon-assisted light harvesting.[9−17] Photosensitive devices utilizing plasmonic nanoantennas generate photocurrent through two dominant mechanisms: near-field photons can be absorbed in a nearby semiconductor to create electron−hole pairs; or high-energy ("hot") electrons generated by the plasmon can tunnel across a semiconductor-metal potential barrier, directly resulting in photocurrent. Plasmonically active devices often have the benefit of being highly polarization-dependent, operational at small biases, and capable of being fabricated with photoactive elements on a scale smaller than the wavelength of the incident light.

Gold "bowtie" nanojunctions, consisting of a nanowire (with or without a nanogap) connected by two extended leads, have been shown to act as combined optical antennas and electrical probes.[18] The plasmon response in this geometry is dominated by a transverse dipolar mode, resonant for incident light polarized perpendicular to the length of the constriction. In devices with nanogaps at their center, made through either electromigration or via a multistep "self-aligned" lithographic technique,[19] the transverse plasmon mode hybridizes with multipolar "dark" modes at the gap edges to form a strong electromagnetic field enhancement at the junction center or "hotspot". The SERS response of molecules assembled into these hotspots follows the signature polarization dependence of dipolar optical antennas, with maximum response perpendicular to the axis of the constriction.[20] This is in contrast to expectations of the nonresonant "lightning rod" effect, when the maximum plasmon response occurs when the incident polarization is parallel to the elongated direction of a metal wire or tip, from the excitation of longitudinal or tip plasmons.[21]

In no-gap bowtie nanowires, resonant laser illumination produces a polarization-dependent hotspot via photothermally induced changes in resistivity.[22] Direct absorption and the excitation of the transverse plasmon mode locally increase the temperature of the nanowire, decreasing its conductance, $-\Delta G$, due to the temperature-dependent resistivity of the metal. The polarization dependence of this change is also dipolar, so that the temperature of the nanowire increases more for the transverse excitation, even without the existence of gap plasmons. This measurement provides a convenient measurement technique to assess the plasmon response of the nanowire material itself.

In this report, we study the photoresponse of bowtie nanoantennas overlaid with a thin Ge film. We examine the plasmon-assisted photoconduction (I_{photo}) in bowties with

Received: May 11, 2015
Published: July 8, 2015

DOI: 10.1021/acsphotonics.5b00250
ACS Photonics 2015, 2, 1192−1198

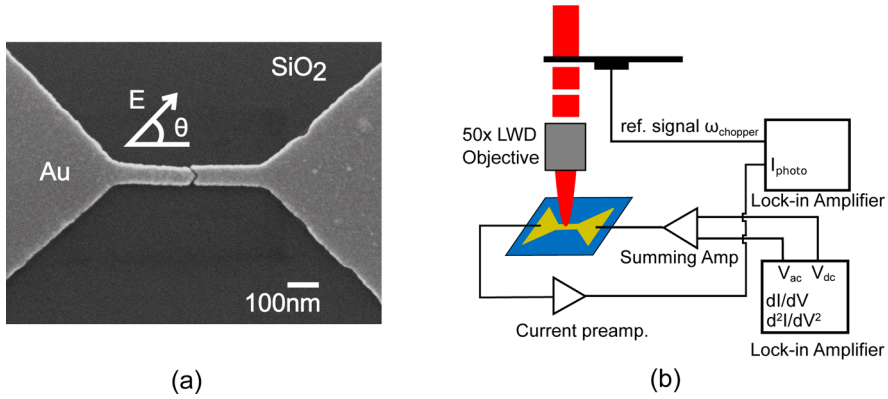

Figure 1. (a) Scanning electron microscope (SEM) image of a typical self-aligned device with 80 ± 5 nm width coated in a 10 nm Ge film. (b) Schematic diagram of the experimental setup. Devices are biased with a dc voltage summed with a small (typically 10 mV) sinusoidal ac excitation voltage. Signal passes through a current preamplifier to two separate lock-in amplifiers, one synched to the ac frequency to measure the first and second harmonic of the differential conductance and a second synched to an optical chopper to measure photoresponse.

nanogaps. At low Ge thicknesses, we find that the photoconductance is maximal with incident polarization transverse to the nanowire; in contrast at higher Ge thicknesses, the maximum photoconductance occurs when the incident polarization is rotated by 90°. The Ge thickness alters which plasmon response is dominant in the nanogaps, the resonant transverse mode (at low thicknesses) or the nonresonant "lightning rod" response (at high thicknesses). A concern is whether the transverse plasmon mode is eliminated entirely due to degradation of the Au properties with thicker Ge layers. To test for this, we also measured the plasmon-induced heating in unbroken (no-gap) nanowires ($-\Delta G$). We find experimentally, and in accord with a computational model, that the presence of Ge predictably redshifts the resonance of the nanoantenna's transverse plasmon mode without degrading the Au plasmonic response. The manipulation of resonant and nonresonant plasmon responses is an interesting avenue to consider in further plasmonic optoelectronic structures.

This work is one of a handful demonstrating plasmon assisted photocurrent in individual nanoantennas. Unlike similar work integrating photosensitive materials, such as graphene,[23,24] MoS_2,[25] and traditional semiconductors,[26−29] into plasmon resonant geometries, the nanogap devices reported in this study rely on a truly nanoscale active optical region, typically 100 nm × 5 nm × 10 nm, fabricated from amorphous Ge, an abundant and easily deposited material. Other schemes for fabricating field enhanced photodetectors and photovoltaic devices have been discussed in depth over the past five years.[3,30−32] This report builds on recent work outlining the strength of nonradiative, hybridized plasmon modes in bowtie nanoantennas.

METHODS

The devices in this report are fabricated on n-type Si wafers with a 200 nm thermally grown oxide layer. Electron beam lithography is used to define the nanowire constriction and small triangular electrodes, which extend to larger, prefabricated Au contact pads deposited using a shadowmask. After development, a 1 nm Ti adhesion layer and 13 nm of Au are deposited by electron beam evaporation, followed by lift-off in acetone. Nanowires are patterned to be 600 nm long and vary from 80 to 140 nm wide, depending on the desired geometry.

In the case of "self-aligned" nanojunctions, an extra step of lithography is needed to create the gap.[19] In the first step, the left half of the nanowire is patterned and the 1 nm/13 nm Ti/Au combination is deposited, followed by a 1 nm layer of SiO_2 and 14 nm layer of Cr. After the metal deposition, exposing the sample to air creates a layer of Cr-oxide which swells to extend just past the edge of the pattern, acting as a shadowmask in the second evaporation. The layer of SiO_2 prevents Cr and unwanted elements of the Cr etchant (namely, cerium) from contaminating the Au and potentially degrading device plasmon response. During a second lithographic step, the right half of the pattern is aligned to the existing left half. An identical evaporation follows with the same materials and thicknesses, to ensure device uniformity. The Cr and SiO_2 are etched away, leaving a 2−10 nm gap between the two sides of the nanowire where the oxidized Cr expanded beyond the first pattern (Figure 1a). The width of the gap can be tailored by adjusting the thickness of the Cr layer.[19]

The devices are cleaned with O_2 plasma and wirebonded to a chip carrier. Each device is scanned with a 785 nm diode laser configured with a telescopic lens rastering system to create a spatial map of the photoresponse. The laser has a Gaussian beam profile with a full width at half-maximum of approximately 1.8 μm, operating in CW mode at a typical laser power of 3−4 mW reaching the sample. A lock-in amplifier, synched to an optical chopper at a frequency of 281 Hz, is used to measure device optical response: either the photocurrent generated in self-aligned devices (I_{photo}) or the optically induced change to the conductance in no-gap nanowires ($\Delta G = \Delta I/V_{dc}$). The sample is biased with the summed output of the desired dc voltage, typically up to 0.2 V, and a 10 mV RMS ac voltage, and a second lock-in, at frequency 789 Hz, measures the first- and second-order differential conductance (dI/dV and d^2I/dV^2). The dc current (I_{dc}) is measured using a digital-to-analog converter (DAC) built into one of the lock-in amplifiers (Figure 1b). After each scan, the laser is then finely positioned at the hotspot center by maximizing I_{photo} or $-\Delta G$, the polarization is rotated continuously from $\theta = 0°$ to $\theta = 360°$ (with $\theta = 0°$ defined to be along the nanoantenna long axis) using a motorized half-wave plate, and the optical and electrical responses are measured. Bare bowtie nanowires (with and without nanogaps) are coated with an amorphous Ge film of varying thickness deposited by electron beam evaporation, and remeasured using the same procedure. All measurements presented in this paper

DOI: 10.1021/acsphotonics.5b00250
ACS Photonics 2015, 2, 1192−1198

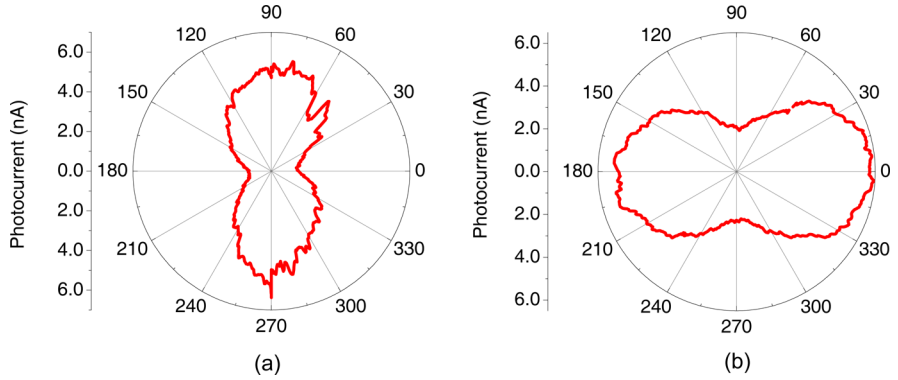

Figure 2. (a) Dipolar polarization dependence of an 80 nm wide nanoantenna with a 10 nm Ge film where the transverse plasmon mode is roughly on resonance with the 785 nm laser. (b) Dipolar polarization of an 130 nm wide nanoantenna with a 35 nm Ge film where the "lightning rod" mode is roughly on resonance with the 785 nm laser.

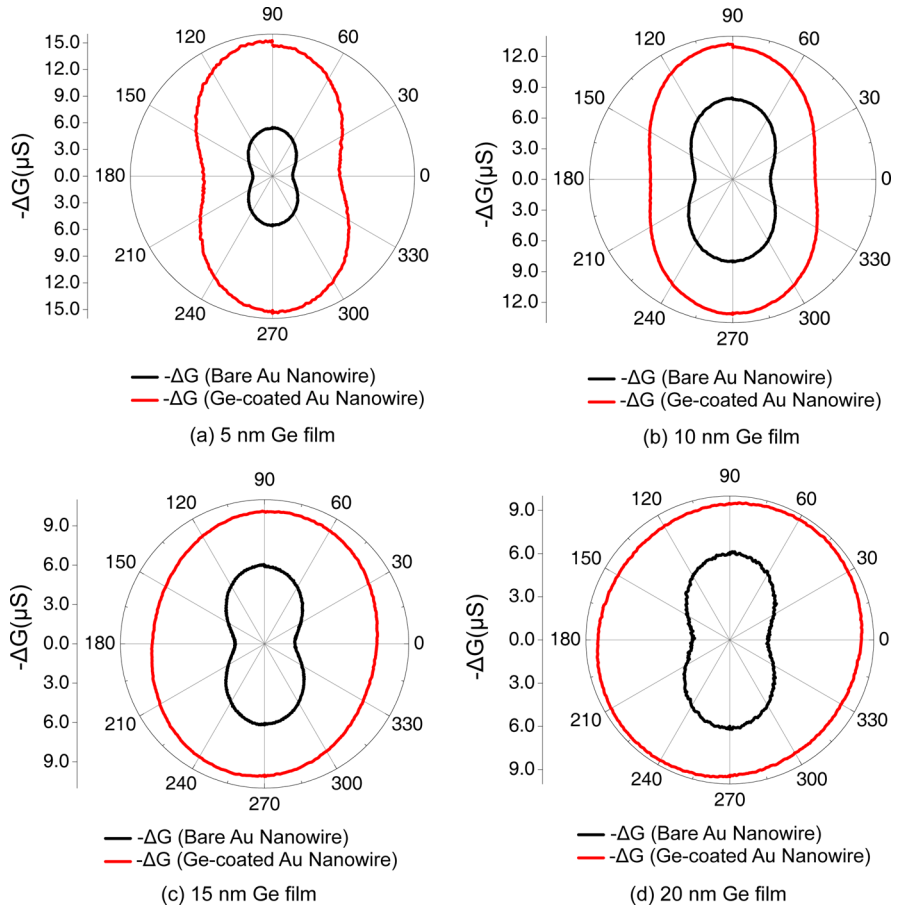

Figure 3. Experimental data displaying the change in polarization dependence for "unbroken" nanowires with varying layers of Ge deposited on top. Each successive trial becomes more circular as the resonance of the transverse mode moves further away from the laser wavelength.

were conducted at room temperature at a pressure on the order of 100 mTorr.

RESULTS

Photoresponse of the self-aligned nanogap junctions is dominated by a positive photoconductance of the Ge in the gap region. Photocurrent measurements of self-aligned nanojunctions present two distinct polarization dependences. In devices with a nanowire width of 80 nm and a 10 nm Ge film, the photocurrent follows the signature dependence of dipolar optical antennas, with maximum response at $\theta = 90°$ (Figure 2a). Repeating this experiment with 130 nm wide nanowire and a thicker layer of Ge (35 nm) shifts the polarization dependence by 90° (Figure 2b). In both cases, photocurrent is linear with respect to laser power and dc bias and only occurs at the junction center.

To understand this, we consider the plasmons in the system. In previous work exploring photoresponse in bowtie nanoantennas, it has been demonstrated that the greatest field enhancement occurs when incident light is polarized perpendicular to the nanowire axis, corresponding to a strong dipolar transverse plasmon mode.[20] For bare Au nanowires, this

DOI: 10.1021/acsphotonics.5b00250
ACS Photonics 2015, 2, 1192−1198

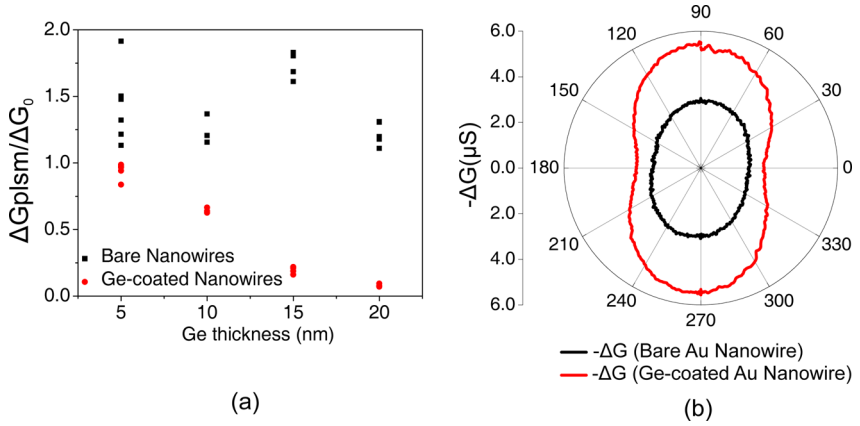

Figure 4. (a) Each point represents the $\Delta G_{plsm}/\Delta G_0$ ratio measured for an individual device, before and after the Ge film deposition. The values for bare nanowires (black squares, with each batch of bare wires marked at the Ge thickness eventually coated) are roughly all the same for all measured bare junctions, which vary in width from device to device. The values for Ge-coated nanowires (red circles) have decreasing $\Delta G_{plsm}/\Delta G_0$ ratios for increasing Ge thickness, indicating that their polar plots are more circular with less contribution of the transverse plasmon mode toward the total photoresponse. (b) Polar plot of an off-resonance, bare device moved closer to resonance with the addition of a 10 nm Ge film. In this case, the $\Delta G_{plsm}/\Delta G_0$ ratio increases.

mode is known to be resonant at 785 nm for bare nanowires ~130 nm wide and 13 nm thick. It would appear that in the narrower-wire nanogap devices with the thinner Ge film, the photocurrent is dominated by this transverse plasmon response, while for the wider-wire nanogap devices with thicker Ge, the dominant plasmon response is that of the nonresonant longitudinal "lightning rod" mode.

An issue is whether, in the thicker Ge devices, the plasmonic properties of the Au itself is degraded (e.g., through partial alloying with the Ge due to the longer deposition) or whether the change in the plasmon response is due purely to shifting of the resonant transverse mode away from the operating wavelength. To understand this dramatic change in nanogap device plasmon response, we fabricate "unbroken" no-gap nanowires and assess the plasmonic properties of the Au through study the photothermally induced change in the conductance, $-\Delta G$ (due to the temperature-dependent Au resistivity), as a function of nanowire width and Ge film thickness. Measurements on bare Au bowtie nanowires (~130 nm wide and 13 nm thick) are consistent with previous work measuring resistive heating in these structures; the conductance change includes a characteristic $\cos^2(\theta)$ polarization-dependent contribution, with a maximum at $\theta = 90°$ due to the contribution to heating from the structure's transverse plasmon mode.[22] This indicates that the laser wavelength is on resonance with the transverse mode of the nanowire (width ~130 nm, thickness 13 nm), heating it approximately by 2−10 K, depending on the exact width of the device and the incident laser power. The increase in temperature can be estimated directly from the change in conductance using the formula provided in Herzog et al. (2014), $\Delta T = \frac{-R^2 \Delta G}{\frac{dR}{dT}}$, where R is the resistance of the device and $\frac{dR}{dT} = 0.12$ for these Au bowtie nanowires. This value has been measured to be consistent for many nanowire devices.

After each initial characterization of bare devices, a Ge film of varying thickness (5, 10, 15, and 20 nm) is deposited by electron beam evaporation and the photoresponse is remeasured (Figure 3). For each trial, the polar plots become progressively more circular, as the increasing thickness of Ge redshifts the resonance of the transverse plasmon mode away from the laser wavelength of 785 nm. The data are fitted to the expression $-\Delta G(\theta) = \Delta G_0 + \Delta G_{plsm} \cos^2(\theta)$. Here, ΔG_0 is the nonresonant, direct absorption contribution, while ΔG_{plsm} is the component of the conductance change due to dipolar plasmon-based heating. The ratio $\Delta G_{plsm}/\Delta G_0$ then gives a measure of the transverse plasmon contribution to the change in conductance for each thickness trial. This ratio is roughly constant for bare junctions across all four trials, but steadily decreases in the presence of increasing Ge film thickness (Figure 4a). By 20 nm of Ge, the devices lose all their polarization dependence; their polar plots become entirely circular, indicating that the presence of the film has shifted the transverse plasmon mode far off-resonance, removing the dipolar response of the nanoantenna and leaving behind only heating from nonresonant absorption.

To verify that the dominant effect on the polarization is redshifting of the plasmon resonance rather than simple attenuation of the plasmon resonance due to Au degradation, we fabricated intentionally off-resonance nanowires, less than 100 nm wide, and then deposited a Ge film to redshift the resonance back to the laser wavelength. The pre- and post-Ge deposition bowties are analyzed following the above procedures (Figure 4b). In this case, we see the $\Delta G_{plsm}/\Delta G_0$ ratio increase, indicating that the polarization dependence of the junction becomes more dipolar in the presence of the Ge film. This effect was found to be consistent in eight measured devices.

These experiments verify that for the gapped nanojunctions a 35 nm Ge film will remove the transverse plasmon mode's contribution toward the photocurrent for a device previously on resonance with the laser wavelength, as seen in Figure 2b. For structures made off resonance with the laser, adding an appropriately thick layer of Ge can tune the device back onto the laser wavelength, as seen in Figure 2a. To map out the appropriate thicknesses of Ge over a range of device widths, the resonance of the transverse plasmon mode in nanoantennas was modeled with a finite-element software package designed to solve differential equations over physical spaces (FEM, COMSOL 3.5a). A cross-sectional model was designed so that the incident light is polarized perpendicular (transverse magnetic mode) to an infinitely long nanowire, isolating the transverse plasmon mode for the purposes of this study (Figure

DOI: 10.1021/acsphotonics.5b00250
ACS Photonics 2015, 2, 1192−1198

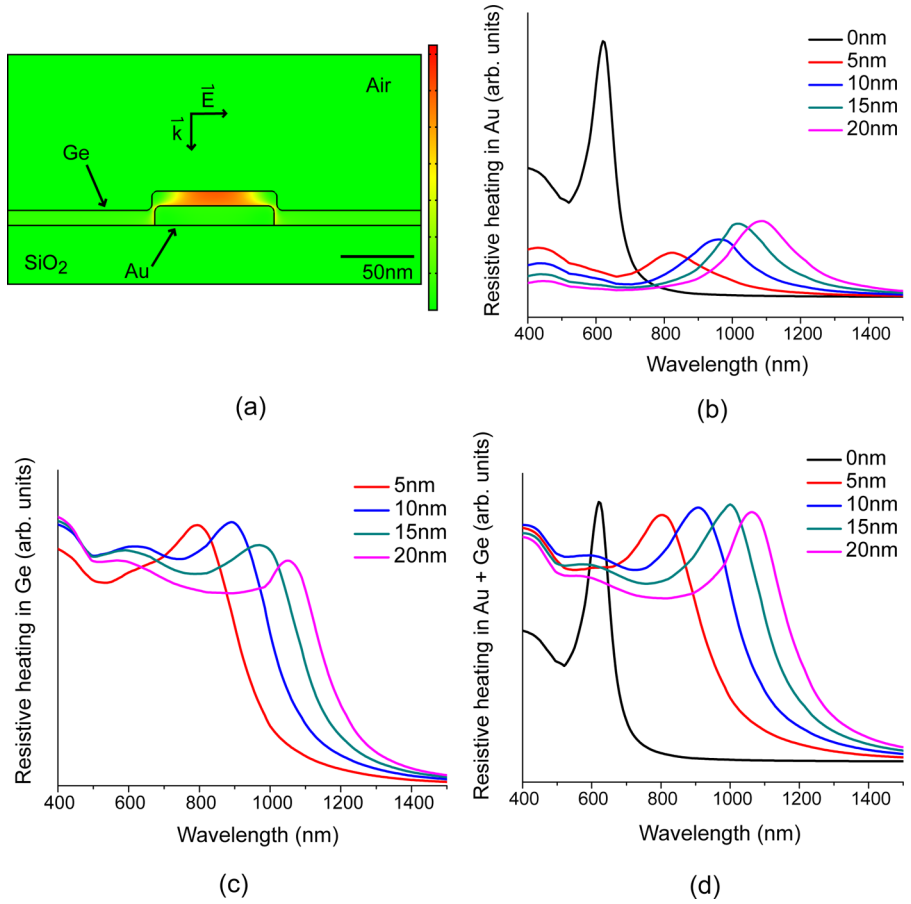

Figure 5. (a) Image of the solution for the variable Q plotted in arbitrary units, green indicating zero heating. (b) Spectra of the variable Q for an 80 nm nanowire in the 2D COMSOL model for varying thicknesses of Ge. (c) Spectra of the variable Q integrated over a portion of the Ge for an 10 nm film on top of an 80 nm nanowire. (d) Spectra of the sum of the resistive heating in the Au nanowire and the Ge film.

5a). Ge is known to be entirely amorphous when deposited by evaporation with the substrate at room temperature, and accordingly, a dielectric function for amorphous Ge was used in the model.[33,34] The dielectric function for Au was taken from Johnson and Christy.[35] Maxwell's equations are solved over the entire solution space as a function of nanowire width and Ge film thickness. For an incident plane wave with free space wavelength ranging from 400 to 1500 nm, a scalar proportional to the optically driven resistive heating is found by integrating resistive heating $Q = \frac{1}{2}\mathrm{Re}(\sigma \|\vec{E}\|^2)$ over the area of the Au, where σ is the electrical conductivity and $\|\vec{E}\|$ is the norm of the total electric field (Figure 5b). As the film thickness increases, the original resonance is red-shifted and broadened, as expected from previous work exploring plasmon modes in the presence of semiconductors.[10,36,37] Bare devices with transverse modes previously resonant at the laser wavelength of 785 nm will be shifted off resonance further into the near-IR in the presence of a 5−10 nm film of Ge.

This simple model provides a proof-of-concept explanation for the shift in the resonance of the transverse plasmon mode, but does not take into account heating from absorption in the Ge layer; it assumes that all photothermally induced change in current comes from heating in the Au alone. This calculational omission accounts for the predicted decrease in the magnitude of the peaks for increasing Ge thickness not seen in the experiment. In contrast, in the measurements the photothermal heating in unbroken bowtie nanowires is larger with the Ge film than without it (i.e., ΔG_0 of the Au is always larger for Ge-coated nanowires than for bare nanowires). Integrating the variable Q over the volume of the Ge film produces a broad plateau at a wavelength below the plasmon resonance due to direct absorption in the Ge overlayer (Figure 5c). Adding the two spectra for Q together (i.e., Figure 5b + c) results in resonance peaks of Ge-coated nanowires with magnitudes for the structure's total optically driven resistive heating comparable to the magnitude of bare junctions (Figure 5d). Extracting precise predictions for the Au temperature increase in Ge-coated nanowires under laser illumination would require knowledge of both the thermal boundary resistance at the interface between the Ge at the Au and the thermal conductance of the amorphous Ge.

DISCUSSION

We have found that the change in polarization response of the photoconductive nanogap antennas with Ge thickness is caused by the tuning of which plasmons dominate at the incident wavelength, the resonant transverse mode, or the nonresonant "lightning rod" response. In either limit we have not addressed the precise mechanism of the positive photoconductance of the Ge-coated nanogap structures. There are several potential mechanisms that could contribute to the photocurrent generated in the Ge-coated nanogap structures: direct absorption of light in the Ge located at the gap creating electron−hole pairs via the photovoltaic effect (PVE); driving "hot" carriers generated in the plasmon across the semi-

DOI: 10.1021/acsphotonics.5b00250
ACS Photonics 2015, 2, 1192−1198

conductor-metal barrier, also known as direct electron transfer (DET); or through plasmon-induced resonant energy transfer (PIRET), where the plasmon can directly excite electron−hole pairs in the Ge.[38,39] Similar studies have also reported photocurrent generation due to the photothermoelectric effect (PTE)[25,40] and optical rectification.[23,41] In this study, photocurrent generation only occurs at the nanojunction center, not along the length of the nanowire, and therefore cannot be due to PTE. Additionally, the photocurrent does not trace the signature nonlinear electrical response for optical rectification, $I_{photo} = \frac{1}{4}\frac{d^2I}{dV^2}V_{ac}^2$. Therefore, the photocarriers in Ge-coated bowtie nanojunctions must be generated by a combination of field-enhanced PVE in the Ge and by plasmonic coupling between the Au and the Ge through DET or PIRET. DET has been reported in various plasmon-based photovoltaic devices, but device responsivity is typically inefficient because collection of hot carriers requires careful engineering of geometry and materials to ensure effective coupling between the plasmon, absorption medium, and electrodes.[11,17,30,32] The measured responsivity in the Ge-coated nanogaps in this work calculated to be $\sim 10^{-6}$ A/W at 0.2 V, which is comparable to the values listed in Shi et al. (2011), who use electromigrated bowtie nanoantennas on top of graphene but is significantly lower than the values reported by Tang et al. (2008). However, their device has a much larger active area and uses crystalline Ge. All three potential mechanisms would have identical polarization dependences; higher fields would produce larger enhancements and more hot carriers, making it difficult to distinguish between these mechanisms based on photoresponse measurements alone. Spectral data or time-resolved measurements could shed light on the relative contribution of each process due to the characteristically short lifetime of hot electrons.

Bowtie nanowires provide a platform for understanding plasmon response in individual metal−semiconductor−metal nanoantennas. We provide experimental and computational evidence that the dominant plasmon modes in such structures may be controlled by tuning between resonant and nonresonant responses. Photocurrent measurements of Ge-coated nanogap structures dominated by the resonant transverse mode are consistent with measurements of unbroken bowtie nanowires; polarization dependence in both cases follows the known $\cos^2(\theta)$ polarization dependence of dipolar optical antennas, with peak photoresponse occurring at an excitation perpendicular to the length of the nanowire (θ = 90°). By optimizing device geometry, this resonant response may be "tuned away" without degrading the Au properties, leaving behind the nonresonant, longitudinal "lightning rod" mode. The nanogap devices operate with a truly nanoscale active region defined by the volume of the interelectrode nanogap. Knowledge of the impact of dielectrics on both resonant and nonresonant local plasmon-enhanced fields is an important step toward fabricating efficient nanoscale light harvesting devices.

AUTHOR INFORMATION

Corresponding Author

*Tel.: (713) 348-3214. E-mail: natelson@rice.edu.

Notes

The authors declare no competing financial interest.

ACKNOWLEDGMENTS

K.M.E. would like to acknowledge Robert A. Welch Foundation Award C-1636 and thank Will Hardy and Yajing Li for useful discussions during the completion of this project. P.Z. and D.N. acknowledge support from ARO Award W911-NF-13-0476.

REFERENCES

(1) Ward, D. R.; Grady, N. K.; Levin, C. S.; Halas, N. J.; Wu, Y.; Nordlander, P.; Natelson, D. Electromigrated Nanoscale Gaps for Surface-Enhanced Raman Spectroscopy. *Nano Lett.* **2007**, *7*, 1396−1400.

(2) Ward, D. R.; Halas, N. J.; Ciszek, J. W.; Tour, J. M.; Wu, Y.; Nordlander, P.; Natelson, D. Simultaneous Measurements of Electronic Conduction and Raman Response in Molecular Junctions. *Nano Lett.* **2008**, *8*, 919−924.

(3) Bharadwaj, P.; Deutsch, B.; Novotny, L. Optical Antennas. *Adv. Opt. Photonics* **2009**, *1*, 438.

(4) Neumann, L.; van 't Oever, J.; van Hulst, N. F. A Resonant Scanning Dipole-Antenna Probe for Enhanced Nanoscale Imaging. *Nano Lett.* **2013**, *13*, 5070−5074.

(5) Zhang, W.; Huang, L.; Santschi, C.; Martin, O. J. F. Trapping and Sensing 10nm Metal Nanoparticles Using Plasmonic Dipole. *Nano Lett.* **2010**, *10*, 1006−1011.

(6) Tsuboi, Y.; Shoji, T.; Kitamura, N.; Takase, M.; Murakoshi, K.; Mizumoto, Y.; Ishihara, H. Optical Trapping of Quantum Dots Based on Gap-Mode-Excitation of Localized Surface Plasmon. *J. Phys. Chem. Lett.* **2010**, *1*, 2327−2333.

(7) Righini, M.; Volpe, G.; Girard, C.; Petrov, D.; Quidant, R. Surface Plasmon Optical Tweezers: Tunable Optical Manipulation in the Femtonewton Range. *Phys. Rev. Lett.* **2008**, *100*, 186804.

(8) Righini, M.; Zelenina, A. S.; Girard, C.; Quidant, R. Parallel and selective trapping in a patterned plasmonic landscape. *Nat. Phys.* **2007**, *3*, 477−480.

(9) Knight, M. W.; Sobhani, H.; Nordlander, P.; Halas, N. J. Photodetection with Active Optical Antennas. *Science* **2011**, *332*, 702−704.

(10) Knight, M. W.; Wang, Y.; Urban, A. S.; Sobhani, A.; Zheng, B. Y.; Nordlander, P.; Halas, N. J. Embedding Plasmonic Nanostructure Diodes Enhances Hot Electron Emission. *Nano Lett.* **2013**, *13*, 1687−1692.

(11) Sobhani, A.; Knight, M. W.; Wang, Y.; Zheng, B.; King, N. S.; Brown, L. V.; Fang, Z.; Nordlander, P.; Halas, N. J. Narrowband photodetection in the near-infrared with a plasmon-induced hot electron device. *Nat. Commun.* **2013**, *4*, 1643.

(12) Sheldon, M. T.; van de Groep, J.; Brown, A. M.; Polman, A.; Atwater, H. A. Plasmoelectric potentials in metal nanostructures. *Science* **2014**, *346*, 828−831.

(13) Li, W.; Valentine, J. Metamaterial Perfect Absorber Based Hot Electron Photodetection. *Nano Lett.* **2014**, *14*, 3510−3514.

(14) Kim, J.-H.; Yeo, J.-S. Enhanced Detection of Broadband Incoherent Light with Nanoridge Plasmonics. *Nano Lett.* **2015**, *15*, 2291−2297.

(15) Collin, S.; Pardo, F.; Bardou, F.; Lemaitre, A.; Averin, S.; Pelouard, J.-L. Harvesting light at the nanoscale by GaAs-gold nanowire arrays. *Opt. Express* **2011**, *19*, 17293−17297.

(16) Balram, K. C.; Audet, R. M.; Miller, D. A. B. Nanoscale resonant-cavity-enhanced germanium photodetectors with lithographically defined spectral response for improved performance at telecommunications wavelengths. *Opt. Express* **2013**, *21*, 10228.

(17) Chalabi, H.; Schoen, D.; Brongersma, M. L. Hot-Electron Photodetection with a Plasmonic Nanostripe Antenna. *Nano Lett.* **2014**, *14*, 1374−1380.

(18) Natelson, D.; Li, Y.; Herzog, J. B. Nanogap structures: combining enhanced Raman spectroscopy and electronic transport. *Phys. Chem. Chem. Phys.* **2013**, *15*, 5262−5275.

(19) Fursina, A.; Lee, S.; Sofin, R. G. S.; Shvets, I. V.; Natelson, D. Nanogaps with very large aspect ratios for electrical measurements. *Appl. Phys. Lett.* **2008**, *92*, 113102.

(20) Herzog, J. B.; Knight, M. W.; Li, Y.; Evans, K. M.; Halas, N. J.; Natelson, D. Dark Plasmons in Hot Spot Generation and Polarization in Interelectrode Nanoscale Junctions. *Nano Lett.* **2013**, *13*, 1359−1364.

DOI: 10.1021/acsphotonics.5b00250
ACS Photonics 2015, 2, 1192−1198

(21) Novotny, L.; Hecht, B. *Principles of Nano-Optics*; Cambridge University Press: Cambridge, U.K., 2006.
(22) Herzog, J. B.; Knight, M. W.; Natelson, D. Thermoplasmonics: Quantifying Plasmonic Heating in Single Nanowires. *Nano Lett.* **2014**, *14*, 499−503.
(23) Shi, S.-F.; Xu, X.; Ralph, D. C.; McEuen, P. L. Plasmon Resonance in Individual Nanogap Electrodes Studied Using Graphene Nanoconstrictions as Photodetectors. *Nano Lett.* **2011**, *11*, 1814−1818.
(24) Gabor, N. M.; Song, J. C. W.; Ma, Q.; Nair, N. L.; Taychatanapat, T.; Watanabe, K.; Taniguchi, T.; Levitov, L. S.; Jarillo-Herrero, P. Hot Carrier-Assisted Intrinsic Photoresponse in Graphene. *Science* **2011**, *334*, 648−652.
(25) Hong, T.; Chamlagain, B.; Hu, S.; Weiss, S. M.; Zhou, Z.; Xu, Y.-Q. Plasmonic Hot Electron Induced Photocurrent Response at MoS_2-Metal Junctions. *ACS Nano* **2015**, *9*, 5357−5363.
(26) Tang, L.; Kocabas, S. E.; Latif, S.; Okyay, A. K.; Ly-Gagnon, D.-S.; Saraswat, K. C.; Miller, D. A. B. Nanometre-scale germanium photodetector enhanced by a near-infrared dipole antenna. *Nat. Photonics* **2008**, *2*, 226−229.
(27) Cao, L.; White, J. S.; Park, J.-S.; Schuller, J. A.; Clemens, B. M.; Brongersma, M. L. Engineering light absorption in semiconductor nanowire devices. *Nat. Mater.* **2009**, *8*, 643−647.
(28) Falk, A. L.; Koppens, F. H. L.; Yu, C. L.; Kang, K.; de Leon Snapp, N.; Akimov, A. V.; Jo, M.-H.; Lukin, M. D.; Park, H. Near-field electrical detection of optical plasmons and single-plasmon sources. *Nat. Phys.* **2009**, *5*, 475−479.
(29) Mousavi, S. S.; Stöhr, A.; Berini, P. Plasmonic photodetector with terahertz electrical bandwidth. *Appl. Phys. Lett.* **2014**, *104*, 143112.
(30) Atwater, H. A.; Polman, A. Plasmonics for improved photovoltaic devices. *Nat. Mater.* **2010**, *9*, 205−213.
(31) Clavero, C. Plasmon-induced hot-electron generation at nanoparticle/metal-oxide interfaces for photovoltaic and photocatalytic devices. *Nat. Photonics* **2014**, *8*, 95−103.
(32) Brongersma, M. L.; Halas, N. J.; Nordlander, P. Plasmon-induced hot carrier science and technology. *Nat. Nanotechnol.* **2015**, *10*, 25−34.
(33) Donovan, T.; Spicer, W.; Bennett, J. M.; Ashley, E. Optical Properties of Amorphous Germanium Films. *Phys. Rev. B* **1970**, *2*, 397−413.
(34) Tomlin, S.; Khawaja, E.; Thutupalli, G. The optical properties of amorphous and crystalline germanium. *J. Phys. C: Solid State Phys.* **1976**, *9*, 4335−4347.
(35) Johnson, P.; Christy, R. Optical Constants of the Noble Metals. *Phys. Rev. B* **1972**, *6*, 4370−4379.
(36) Knight, M. W.; Wu, Y.; Lassiter, J. B.; Nordlander, P.; Halas, N. J. Substrates Matter: Influence of an Adjacent Dielectric on an Individual Plasmonic Nanoparticle. *Nano Lett.* **2009**, *9*, 2188−2192.
(37) Liu, N.; Tang, M. L.; Hentschel, M.; Giessen, H.; Alivisatos, A. P. Nanoantenna-enhanced gas sensing in a single tailored nanofocus. *Nat. Mater.* **2011**, *10*, 631−636.
(38) Cushing, S. K.; Li, J.; Meng, F.; Senty, T. R.; Suri, S.; Zhi, M.; Li, M.; Bristow, A. D.; Wu, N. Photocatalytic Activity Enhanced by Plasmonic Resonant Energy Transfer from Metal to Semiconductor. *J. Am. Chem. Soc.* **2012**, *134*, 15033−15041.
(39) Li, G.; Cherqui, C.; Bigelow, N. W.; Duscher, G.; Straney, P. J.; Millstone, J. E.; Masiello, D. J.; Camden, J. P. Spatially Mapping Energy Transfer from Single Plasmonic Particles to Semiconductor Substrates via STEM/EELS. *Nano Lett.* **2015**, *15*, 3465−3471.
(40) Echtermeyer, T. J.; Nene, P. S.; Trushin, M.; Gorbachev, R. V.; Eiden, A. L.; Milana, S.; Sun, Z.; Schliemann, J.; Lidorikis, E.; Novoselov, K. S.; Ferrari, A. Photothermoelectric and Photoelectric Contributions to Light Detection in Metal-Graphene-Metal Photodetectors. *Nano Lett.* **2014**, *14*, 3733−3742.
(41) Ward, D. R.; Hüser, F.; Pauly, F.; Cuevas, J. C.; Natelson, D. Optical rectification and field enhancement in a plasmonic nanogap. *Nat. Nanotechnol.* **2010**, *5*, 732−736.

DOI: 10.1021/acsphotonics.5b00250
ACS Photonics 2015, 2, 1192−1198